Available online at www.sciencedirect.com
SCIENCE DIRECT®
Journal of Sound and Vibration 282 (2005) 781–804
JOURNAL OF SOUND AND VIBRATION
www.elsevier.com/locate/jsvi

Exact solution for the vibration and active damping of composite plates with piezoelectric shear actuators

Brian P. Baillargeon, Senthil S. Vel*

Department of Mechanical Engineering, University of Maine, 5711 Boardman Hall, Room 214, Orono, ME 04469-5711, USA

Received 15 August 2003; accepted 13 March 2004

Abstract

An exact three-dimensional solution is obtained for the cylindrical bending vibration of simply supported laminated composite plates with an embedded piezoelectric shear actuator. The piezoelectric actuator, which is poled in the longitudinal direction, will induce a transverse shear strain in the hybrid laminate when it is subjected to an electric field in the thickness direction. Suitable displacement and electric potential functions that identically satisfy the boundary conditions at the simply supported edges are used to reduce the equations that govern the steady-state vibrations of the hybrid laminate to a set of coupled ordinary differential equations, which are solved by employing the power series method. Natural frequencies, mode shapes, displacements, electric potential and stresses are presented for three-layer hybrid laminates consisting of a piezoelectric shear actuator sandwiched between fiber-reinforced composite layers. Active vibration damping is implemented using either a position feedback controller or velocity feedback controller. Frequency response curves for different controller frequencies, controller damping ratio and feedback gain demonstrate that the embedded shear actuator can be used for active damping of the fundamental flexural mode. In addition, it is shown that vibration suppression of thickness modes is also feasible using a shear actuator.

*Corresponding author. Tel.: +1-207-581-2777; fax: +1-207-581-2379.
E-mail address: senthil.vel@maine.edu (S.S. Vel).

0022-460X/$ - see front matter © 2004 Elsevier Ltd. All rights reserved.
doi:10.1016/j.jsv.2004.03.042

1. Introduction

More than a decade of intensive research in the area of smart/adaptive structures has demonstrated the viability and potential of this technology. A class of smart structures, consisting of piezoelectric materials integrated with structural systems, has found widespread use in engineering applications. Numerous applications have been proposed and conceived experimentally, such as for active vibration suppression [1–3], noise cancellation [4,5] and shape control [6,7].

A piezoelectric actuator in an adaptive structure is a thin rectangular element that is generally poled in the thickness direction and is usually bonded to the surfaces of the host structure. The application of an electric field in the thickness direction causes the actuator's lateral dimensions to increase or decrease. The lateral deformations of the actuator force the host structure to deform. In order to successfully incorporate piezoelectric actuators into a structure, the mechanical interaction between the actuators and the host structure must be fully understood. Several mechanical models and finite-element studies have been presented for hybrid beams and plates with thickness-poled actuators [8–12]. Ray et al. [13] and Heyliger and Brooks [14] have obtained exact three-dimensional solutions for the static cylindrical bending of simply supported piezoelectric laminates. Exact solutions for simply supported rectangular piezoelectric laminates were given by Heyliger [15,16], Bisegna and Maceri [17], and Lee and Jiang [18]. A similar technique was employed by Yang et al. [19] and Batra et al. [20] to analyze the vibrations of a simply supported plate with piezoceramic actuators either bonded to its upper and lower surfaces or embedded within the laminate. Vel and Batra [21–23] have derived three-dimensional analytical solutions for thick piezoelectric plates subjected to arbitrary boundary conditions at the edges. Heyliger and Brooks [24] and Heyliger and Saravanos [25] have presented exact solutions for the free vibration of hybrid plates with thickness-poled piezoelectric layers.

Piezoelectric actuators poled in the thickness direction are usually placed at the extreme thickness positions of a plate-like structure to achieve the most effective actuation. This subjects the actuators to high longitudinal stresses that may be detrimental to the brittle piezoceramic material. Furthermore, surface-bonded actuators are likely to be damaged by contact with surrounding objects. To alleviate these problems Sun and Zhang [26] proposed an adaptive sandwich structure consisting of an axially poled piezoelectric core sandwiched between two elastic facing sheets. The application of an electric field in the thickness direction will induce transverse shear deformation of the core, thus generating the desired transverse deflection of the sandwich structure. Piezoelectric actuators poled in such a way as to produce transverse shear deformation under the action of an electric field in the thickness direction are called *shear actuators*. Piezoceramic thin actuators poled along a line in the plane of the actuator were studied by Boriseiko et al. [27]. Piezoelectric shear actuators of various dimensions are commercially available [28]. Zhang and Sun [29,30] developed a beam theory for sandwich structures containing shear actuators by modeling the facing sheets as classical Euler–Bernoulli beams and the central core as a Timoshenko beam which allows transverse shear deformation. Benjeddou et al. [31] developed a unified finite-element model for extension and shear actuation mechanisms with more detailed formulation of the electric problem. Theoretical and finite-element models for the vibration control of sandwich beams with shear actuators have demonstrated that shear actuators can be more effective than thickness-poled actuators for the control of bending vibrations [32].

Benjeddou and Deü [33] have analyzed the vibration of a piezoelectric sandwich plate using a layer-wise first-order shear deformation theory and through-thickness quadratic electric profile. Trindade and Benjeddou [34] have reviewed various hybrid active–passive damping treatments using viscoelastic and piezoelectric materials. Batra and Geng [35] have compared the performance of axially-poled shear actuators and thickness-poled extension actuators for the active constrained layer damping of adaptive structures.

The exact solutions for the vibration of composite plates with thickness-poled piezoelectric extension actuators given by Heyliger and Brooks [24] and Heyliger and Saravanos [25] are not applicable to piezoelectric shear actuators since they assume that the only nonzero components of the piezoelectric tensor in the contracted notation (see Eq. (2) below) are $e_{31}, e_{32}, e_{33}, e_{24}$ and e_{15}. However, for a piezoelectric shear actuator with poling axis **P** at an angle to the x_1-axis in the x_1–x_2 plane (Fig. 1), the nonzero components of the piezoelectric tensor in the contracted notation are $e_{11}, e_{12}, e_{13}, e_{16}, e_{21}, e_{22}, e_{23}, e_{26}, e_{34}$ and e_{35}. Recently, Vel and Batra [36,37] gave an exact solution for the static bending of a simply supported sandwich plate with an embedded piezoelectric shear actuator.

Here we derive an exact solution for the cylindrical bending vibration of composite plates with embedded piezoelectric shear actuators. The equations of motion, charge equation and constitutive equations of linear piezoelectricity are exactly satisfied at every point in the laminate. The boundary conditions at the simply supported edges, the traction boundary conditions on the top and bottom surfaces and the electromechanical continuity conditions at the interfaces between dissimilar layers are also exactly satisfied. The first 12 natural frequencies, mode shapes and through-the-thickness plots of the displacements and stresses are presented for sandwich plates consisting of axially poled piezoelectric cores sandwiched between two elastic surface layers. Active vibration damping is implemented using either a positive position feedback (PPF) controller [38–40] or a velocity feedback controller, wherein a second-order compensator is forced by either the transverse displacement or velocity response of the structure. The controller coordinate, magnified by a gain, is then fed back as a voltage input to a piezoelectric shear actuator. Frequency-response curves for different controller frequencies, controller damping ratio and feedback gain demonstrate that the embedded shear actuator can be used for active damping

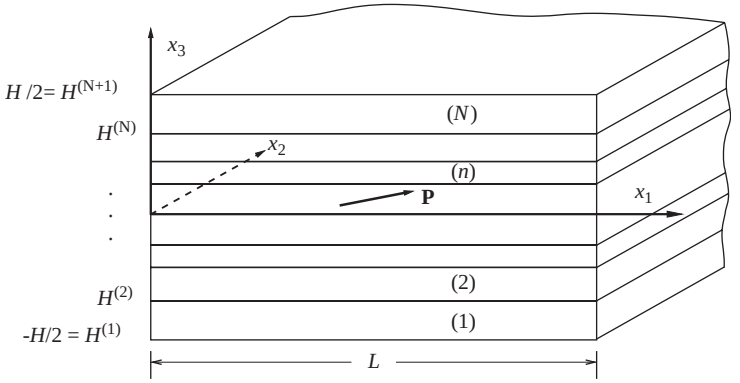

Fig. 1. N-layer laminated piezoelectric plate.

of the fundamental flexural mode. Vibration suppression of the thickness modes can also be achieved using the shear actuator.

2. Formulation of the problem

We use a rectangular Cartesian coordinate system, shown in Fig. 1, to describe the infinitesimal deformations of an N-layer piezoelectric laminated rectangular plate occupying the region $[0, L] \times (-\infty, \infty) \times [-H/2, H/2]$ in the unstressed reference configuration. The laminate is of infinite extent in the x_2-direction. The vertical positions of the bottom and top surfaces as well as of the $N-1$ interfaces between the adjoining laminae are denoted by $H^{(1)} = -H/2, H^{(2)}, \ldots, H^{(n)}, \ldots, H^{(N)}, H^{(N+1)} = H/2$. Each lamina is assumed to be made of a homogeneous material.

The equations of motion for lamina n, in the absence of body forces and free charges, are

$$\sigma_{ij,j}^{(n)} = \rho^{(n)} \ddot{u}_i^{(n)}, \quad D_{j,j}^{(n)} = 0, \quad (i,j = 1,2,3), \tag{1}$$

where σ_{ij}, u_i and D_j are the components of the Cauchy stress tensor, displacement vector and electric displacement vector, respectively, and ρ is the mass density. A comma followed by index j indicates partial differentiation with respect to the present position x_j of a material particle, a repeated index implies summation over the range of the index, a superimposed dot indicates differentiation with respect to time t and the superscript (n) signifies quantities for lamina n.

The elastic and piezoelectric materials of the hybrid laminate are assumed to be monoclinic materials of class m with the x_3-plane being the symmetry plane [41]. Fiber-reinforced composite materials and piezoelectric materials with principal material axis in the x_1–x_2 plane (Fig. 1) belong to the group of monoclinic materials of crystal class m. The constitutive equations, in contracted notation, for lamina n are

$$\begin{Bmatrix} \sigma_{11} \\ \sigma_{22} \\ \sigma_{33} \\ \sigma_{23} \\ \sigma_{31} \\ \sigma_{12} \end{Bmatrix}^{(n)} = \begin{bmatrix} C_{11} & C_{12} & C_{13} & 0 & 0 & C_{16} \\ C_{12} & C_{22} & C_{23} & 0 & 0 & C_{26} \\ C_{13} & C_{23} & C_{33} & 0 & 0 & C_{36} \\ 0 & 0 & 0 & C_{44} & C_{45} & 0 \\ 0 & 0 & 0 & C_{45} & C_{55} & 0 \\ C_{16} & C_{26} & C_{36} & 0 & 0 & C_{66} \end{bmatrix}^{(n)} \begin{Bmatrix} \varepsilon_{11} \\ \varepsilon_{22} \\ \varepsilon_{33} \\ 2\varepsilon_{23} \\ 2\varepsilon_{31} \\ 2\varepsilon_{12} \end{Bmatrix}^{(n)} - \begin{bmatrix} e_{11} & e_{21} & 0 \\ e_{12} & e_{22} & 0 \\ e_{13} & e_{23} & 0 \\ 0 & 0 & e_{34} \\ 0 & 0 & e_{35} \\ e_{16} & e_{26} & 0 \end{bmatrix}^{(n)} \begin{Bmatrix} E_1 \\ E_2 \\ E_3 \end{Bmatrix}^{(n)},$$

$$\begin{Bmatrix} D_1 \\ D_2 \\ D_3 \end{Bmatrix}^{(n)} = \begin{bmatrix} e_{11} & e_{12} & e_{13} & 0 & 0 & e_{16} \\ e_{21} & e_{22} & e_{23} & 0 & 0 & e_{26} \\ 0 & 0 & 0 & e_{34} & e_{35} & 0 \end{bmatrix}^{(n)} \begin{Bmatrix} \varepsilon_{11} \\ \varepsilon_{22} \\ \varepsilon_{33} \\ 2\varepsilon_{23} \\ 2\varepsilon_{31} \\ 2\varepsilon_{12} \end{Bmatrix}^{(n)} + \begin{bmatrix} \epsilon_{11} & \epsilon_{12} & 0 \\ \epsilon_{12} & \epsilon_{22} & 0 \\ 0 & 0 & \epsilon_{33} \end{bmatrix}^{(n)} \begin{Bmatrix} E_1 \\ E_2 \\ E_3 \end{Bmatrix}^{(n)}, \tag{2}$$

where ε_{ij} are the components of the infinitesimal strain tensor, E_j the electric field, C_{ij} the elasticity constants, e_{ij} the piezoelectric moduli and ϵ_{ij} the electric permittivity. Material elasticities and permittivities are assumed to yield a positive stored energy density for every nonrigid deformation and/or nonzero electric field [42]. For an elastic layer, the piezoelectric moduli e_{ij} are identically zero. The infinitesimal strain tensor and the electric field are related to the mechanical displacements u_j and the electric potential ϕ by

$$\varepsilon_{ij}^{(n)} = \frac{1}{2}(u_{i,j}^{(n)} + u_{j,i}^{(n)}), \quad E_j^{(n)} = -\phi_{,j}^{(n)}. \tag{3}$$

The edges $x_1 = 0$ and L are assumed to be mechanically simply supported and electrically insulated; that is

$$\sigma_{11}^{(n)} = \sigma_{12}^{(n)} = 0, \quad u_3^{(n)} = 0, \quad D_1^{(n)} = 0 \quad \text{at } x_1 = 0, L. \tag{4}$$

The mechanical boundary conditions of a simply supported plate for the stresses and displacements in Eq. (4) are identical to those assumed by Pagano [43] and Heyliger and Brooks [24]. Exact three-dimensional solutions for laminated plates can be obtained only for certain combinations of boundary conditions on the edges. Heyliger and Brooks [24] considered electrically grounded ($\phi^{(n)} = 0$) edges at $x_1 = 0, L$ in order to obtain exact solutions for laminates with thickness-poled piezoelectric actuators. In the case of piezoelectric shear actuators, we assume that the edges are electrically insulated ($D_1^{(n)} = 0$) in order to obtain an exact solution [36].

The boundary conditions prescribed on the top and bottom surfaces of the laminate consist of either a mechanical displacement component u_m or the corresponding traction component σ_{3m}, and either the electric potential ϕ or the normal component of the electric displacement D_3. Typically nonzero normal tractions and electric potential are prescribed on the top and bottom surfaces of a plate. Since any function can be expanded in terms of a Fourier series, it is sufficient to consider electrical and/or mechanical loads on the top surface of the form

$$\begin{aligned} &\sigma_{33}(x_1, H/2) = q_0 \, e^{i\omega t} \sin\tfrac{k\pi x_1}{L}, \quad \sigma_{31}(x_1, H/2) = \sigma_{32}(x_1, H/2) = 0, \\ &\phi(x_1, H/2) = \phi_0 \, e^{i\omega t} \cos\tfrac{k\pi x_1}{L}, \end{aligned} \tag{5}$$

where k is a nonnegative integer and ω denotes the angular frequency. Similar boundary conditions are specified on the bottom surface of the laminate.

The interface conditions on the material surfaces $x_3 = H^{(2)}, \ldots, H^{(N)}$ may be specified as follows:

(1) If the surface $x_3 = H^{(n+1)}$ is an interface between two laminae, the mechanical displacements, surface tractions, the electric potential and the normal component of the electric displacement between them are continuous. That is

$$u_j^{(n)} = u_j^{(n+1)}, \quad \sigma_{3j}^{(n)} = \sigma_{3j}^{(n+1)}, \quad \phi^{(n)} = \phi^{(n+1)}, \quad D_3^{(n)} = D_3^{(n+1)} \quad \text{on } x_3 = H^{(n+1)}. \tag{6}$$

Thus, the adjoining laminae are presumed to be mechanically and electrically perfectly bonded together.

(2) If the interface $x_3 = H^{(n+1)}$ is electroded, then the electric potential on this surface is assumed to be a known function of the form $\phi_0^{(n+1)} \cos k\pi x_1/L$. The normal component of the electric displacement need not be continuous across this interface. Thus

$$u_j^{(n)} = u_j^{(n+1)}, \quad \sigma_{3j}^{(n)} = \sigma_{3j}^{(n+1)}, \quad \phi^{(n)} = \phi^{(n+1)} = \phi_0^{(n+1)} e^{i\omega t} \cos k\pi x_1/L \quad \text{on } x_3 = H^{(n+1)}. \tag{7}$$

3. Exact solution

We postulate that the displacements $u_j^{(n)}$ and electric potential $\phi^{(n)}$ are functions of x_1 and x_3 only. Thus the laminate is in a generalized plane strain state of deformation. This assumption is reasonable because the applied loads and material properties are independent of x_2, and the body is of infinite extent in the x_2-direction.

We seek a semi-inverse solution by assuming the following forms for the displacements and electric potential:

$$\begin{aligned}
u_1^{(n)}(x_1, x_3, t) &= U_1^{(n)}(x_3) e^{i\omega t} \cos px_1, \\
u_2^{(n)}(x_1, x_3, t) &= U_2^{(n)}(x_3) e^{i\omega t} \cos px_1, \\
u_3^{(n)}(x_1, x_3, t) &= U_3^{(n)}(x_3) e^{i\omega t} \sin px_1, \\
\phi^{(n)}(x_1, x_3, t) &= \Phi^{(n)}(x_3) e^{i\omega t} \cos px_1,
\end{aligned} \tag{8}$$

where $p = k\pi/L$. The assumed displacement field for u_3 satisfies the boundary conditions (4) at the edges $x_1 = 0,\ L$.

Substitution of Eqs. (8) into Eqs. (3) and the result into Eqs. (2) yields the following expressions for the stresses and electric displacements:

$$\begin{aligned}
\sigma_{11}^{(n)} &= (-C_{11}^{(n)} U_1^{(n)} p + C_{13}^{(n)} (U_3^{(n)})' - C_{16}^{(n)} U_2^{(n)} p - e_{11}^{(n)} \Phi^{(n)} p) \sin px_1, \\
\sigma_{22}^{(n)} &= (-C_{12}^{(n)} U_1^{(n)} p + C_{23}^{(n)} (U_3^{(n)})' - C_{26}^{(n)} U_2^{(n)} p - e_{12}^{(n)} \Phi^{(n)} p) \sin px_1, \\
\sigma_{33}^{(n)} &= (-C_{13}^{(n)} U_1^{(n)} p + C_{33}^{(n)} (U_3^{(n)})' - C_{36}^{(n)} U_2^{(n)} p - e_{13}^{(n)} \Phi^{(n)} p) \sin px_1, \\
\sigma_{23}^{(n)} &= (C_{44}^{(n)} (U_2^{(n)})' + C_{45}^{(n)} (U_1^{(n)})' + C_{45}^{(n)} U_3^{(n)} p + e_{34}^{(n)} (\Phi^{(n)})') \cos px_1, \\
\sigma_{31}^{(n)} &= (C_{45}^{(n)} (U_2^{(n)})' + C_{55}^{(n)} (U_1^{(n)})' + C_{55}^{(n)} U_3^{(n)} p + e_{35}^{(n)} (\Phi^{(n)})') \cos px_1, \\
\sigma_{12}^{(n)} &= (-C_{16}^{(n)} U_1^{(n)} p + C_{36}^{(n)} (U_3^{(n)})' - C_{66}^{(n)} U_2^{(n)} p - e_{16}^{(n)} \Phi^{(n)} p) \sin px_1, \\
D_1^{(n)} &= (-e_{11}^{(n)} U_1^{(n)} p + e_{13}^{(n)} (U_3^{(n)})' - e_{16}^{(n)} U_2^{(n)} p + \epsilon_{11}^{(n)} \Phi^{(n)} p) \sin px_1, \\
D_2^{(n)} &= (-e_{21}^{(n)} U_1^{(n)} p + e_{23}^{(n)} (U_3^{(n)})' - e_{26}^{(n)} U_2^{(n)} p + \epsilon_{12}^{(n)} \Phi^{(n)} p) \sin px_1, \\
D_3^{(n)} &= (e_{34}^{(n)} (U_2^{(n)})' + e_{35}^{(n)} (U_1^{(n)})' + e_{35}^{(n)} U_3^{(n)} p - \epsilon_{33}^{(n)} (\Phi^{(n)})') \cos px_1,
\end{aligned} \tag{9}$$

where the prime denotes derivative with respect to x_3. An examination of Eq. (9) reveals that the stress components σ_{11} and σ_{12} and the electric displacement D_1 satisfy the boundary conditions at the edges $x_1 = 0$ and L.

Substitution of Eqs. (9) into the governing Eqs. (1) yields four coupled second-order ordinary differential equations for $U_j^{(n)}(x_3)$ and $\Phi^{(n)}(x_3)$,

$$\begin{aligned}
&-C_{11}^{(n)}U_1^{(n)}p^2+(C_{13}^{(n)}+C_{55}^{(n)})(U_3^{(n)})'p-C_{16}^{(n)}U_2^{(n)}p^2-e_{11}^{(n)}\Phi^{(n)}p^2+C_{45}^{(n)}(U_2^{(n)})''\\
&\quad+C_{55}^{(n)}(U_1^{(n)})''+e_{35}^{(n)}(\Phi^{(n)})''=-\rho^{(n)}\omega^2U_1^{(n)},\\
&-C_{16}^{(n)}U_1^{(n)}p^2+(C_{36}^{(n)}+C_{45}^{(n)})(U_3^{(n)})'p-C_{66}^{(n)}U_2^{(n)}p^2-e_{16}^{(n)}\Phi^{(n)}p^2+C_{44}^{(n)}(U_2^{(n)})''\\
&\quad+C_{45}^{(n)}(U_1^{(n)})''+e_{34}^{(n)}(\Phi^{(n)})''=-\rho^{(n)}\omega^2U_2^{(n)},\\
&-(C_{13}^{(n)}+C_{55}^{(n)})(U_1^{(n)})'p-(C_{36}^{(n)}+C_{45}^{(n)})(U_2^{(n)})'p-C_{55}^{(n)}U_3^{(n)}p^2-(e_{13}^{(n)}+e_{35}^{(n)})(\Phi^{(n)})'p\\
&\quad+C_{33}^{(n)}(U_3^{(n)})=-\rho^{(n)}\omega^2U_3^{(n)},\\
&-e_{11}^{(n)}U_1^{(n)}p^2+(e_{13}^{(n)}+e_{35}^{(n)})(U_3^{(n)})'p-e_{16}^{(n)}U_2^{(n)}p^2+\epsilon_{12}^{(n)}\Phi^{(n)}p^2+e_{34}^{(n)}(U_2^{(n)})''\\
&\quad+e_{35}^{(n)}(U_1^{(n)})''-\epsilon_{33}^{(n)}(\Phi^{(n)})''=0.
\end{aligned}\tag{10}$$

We assume a power series solution for $U_i^{(n)}(x_3)$ and $\Phi^{(n)}(x_3)$ [44]:

$$U_i^{(n)}(x_3)=\sum_{\beta=0}^{\infty}\tilde{U}_i^{(n,\beta)}x_3^{\beta},\quad \Phi^{(n)}(x_3)=\sum_{\beta=0}^{\infty}\tilde{\Phi}^{(n,\beta)}x_3^{\beta}.\tag{11}$$

Inserting Eqs. (11) into the differential equations (10) shifting the summation index, β, to range over zero to infinity and equating like powers of x_3 on both sides of the equations results in the following recurrence relations for the series coefficients:

$$\begin{Bmatrix}\tilde{U}_1^{(n,\beta+2)}\\ \tilde{U}_2^{(n,\beta+2)}\\ \tilde{U}_3^{(n,\beta+2)}\\ \tilde{\Phi}^{(n,\beta+2)}\end{Bmatrix}=\frac{1}{(\beta+2)(\beta+1)}(\mathbf{K}^{(n)})^{-1}\mathbf{A}^{(n)}\begin{Bmatrix}\tilde{U}_1^{(n,\beta)}\\ \tilde{U}_2^{(n,\beta)}\\ \tilde{U}_3^{(n,\beta)}\\ \tilde{\Phi}^{(n,\beta)}\end{Bmatrix}+\frac{1}{(\beta+2)}(\mathbf{K}^{(n)})^{-1}\mathbf{B}^{(n)}\begin{Bmatrix}\tilde{U}_1^{(n,\beta+1)}\\ \tilde{U}_2^{(n,\beta+1)}\\ \tilde{U}_3^{(n,\beta+1)}\\ \tilde{\Phi}^{(n,\beta+1)}\end{Bmatrix},\tag{12}$$

where

$$\mathbf{K}^{(n)}=\begin{bmatrix}C_{55}^{(n)} & C_{45}^{(n)} & 0 & e_{35}^{(n)}\\ C_{45}^{(n)} & C_{44}^{(n)} & 0 & e_{34}^{(n)}\\ 0 & 0 & C_{33}^{(n)} & 0\\ e_{35}^{(n)} & e_{34}^{(n)} & 0 & -\epsilon_{33}^{(n)}\end{bmatrix},\tag{13}$$

$$\mathbf{A}^{(n)}=\begin{bmatrix}C_{11}^{(n)}p^2-\rho^{(n)}\omega^2 & C_{16}^{(n)}p^2 & 0 & e_{11}^{(n)}p^2\\ C_{16}^{(n)}p^2 & C_{66}^{(n)}p^2-\rho^{(n)}\omega^2 & 0 & e_{16}^{(n)}p^2\\ 0 & 0 & C_{55}^{(n)}p^2-\rho^{(n)}\omega^2 & 0\\ e_{11}^{(n)}p^2 & e_{16}^{(n)}p^2 & 0 & -\epsilon_{11}^{(n)}p^2\end{bmatrix},\tag{14}$$

$$\mathbf{B}^{(n)} = \begin{bmatrix} 0 & 0 & -(C_{13}^{(n)} + C_{55}^{(n)})p & 0 \\ 0 & 0 & -(C_{36}^{(n)} + C_{45}^{(n)})p & 0 \\ (C_{13}^{(n)} + C_{55}^{(n)})p & (C_{36}^{(n)} + C_{45}^{(n)})p & 0 & (e_{13}^{(n)} + e_{35}^{(n)})p \\ 0 & 0 & -(e_{13}^{(n)} + e_{35}^{(n)})p & 0 \end{bmatrix}. \tag{15}$$

The series coefficients $\tilde{U}_i^{(n,\beta+2)}$ and $\tilde{\Phi}^{(n,\beta+2)}$ for $\beta > 0$ can be written in terms of eight unknown coefficients for each lamina, namely $\tilde{U}_1^{(n,0)}$, $\tilde{U}_2^{(n,0)}$, $\tilde{U}_3^{(n,0)}$, $\tilde{\Phi}^{(n,0)}$, $\tilde{U}_1^{(n,1)}$, $\tilde{U}_2^{(n,1)}$, $\tilde{U}_3^{(n,1)}$ and $\tilde{\Phi}^{(n,1)}$, using the recurrence relations (12). Therefore, there are $8N$ unknown coefficients for an N-layer composite laminate. These coefficients are determined by satisfying four boundary conditions on the top surface, four conditions on the bottom surface of the laminate (5) and eight interface conditions (6) or (7) at each of the $(N-1)$ interfaces.

3.1. Free vibration analysis

The simply supported plate is in a state of free vibration if it is not subjected to any applied mechanical or electric loads. For fixed k (i.e. fixed p), the recurrence relations (12) are evaluated successively for $\beta = 0, 1, 2, \ldots$, to obtain $\tilde{U}_1^{(n,\beta+2)}$, $\tilde{U}_2^{(n,\beta+2)}$, $\tilde{U}_3^{(n,\beta+2)}$ and $\tilde{\Phi}^{(n,\beta+2)}$ in terms of eight arbitrary constants $\tilde{U}_1^{(n,0)}$, $\tilde{U}_2^{(n,0)}$, $\tilde{U}_3^{(n,0)}$, $\tilde{\Phi}^{(n,0)}$, $\tilde{U}_1^{(n,1)}$, $\tilde{U}_2^{(n,1)}$, $\tilde{U}_3^{(n,1)}$, $\tilde{\Phi}^{(n,1)}$ and the angular frequency ω as

$$\begin{aligned} \tilde{U}_i^{(n,\beta+2)} &= \sum_{j=1}^{3} \left[a_{ij}^{(n,\beta+2)}(\omega)\tilde{U}_j^{(n,0)} + \hat{a}_{ij}^{(n,\beta+2)}(\omega)\tilde{U}_j^{(n,1)} \right] + b_i^{(n,\beta+2)}(\omega)\tilde{\Phi}^{(n,0)} + \hat{b}_i^{(n,\beta+2)}(\omega)\tilde{\Phi}^{(n,1)}, \\ \tilde{\Phi}^{(n,\beta+2)} &= \sum_{j=1}^{3} \left[q_j^{(n,\beta+2)}(\omega)\tilde{U}_j^{(n,0)} + \hat{q}_j^{(n,\beta+2)}(\omega)\tilde{U}_j^{(n,1)} \right] + r^{(n,\beta+2)}(\omega)\tilde{\Phi}^{(n,0)} + \hat{r}^{(n,\beta+2)}(\omega)\tilde{\Phi}^{(n,1)}. \end{aligned} \tag{16}$$

Here, $a_{ij}^{(n,\beta+2)}(\omega)$, $\hat{a}_{ij}^{(n,\beta+2)}(\omega)$, $b_i^{(n,\beta+2)}(\omega)$, $\hat{b}_i^{(n,\beta+2)}(\omega)$, $q_j^{(n,\beta+2)}(\omega)$, $\hat{q}_j^{(n,\beta+2)}(\omega)$, $r^{(n,\beta+2)}(\omega)$ and $\hat{r}^{(n,\beta+2)}(\omega)$ are known polynomials of ω. The degree of the polynomials increases with increasing β due to the recurrence relations. Substitution of Eqs. (16) and (11) into Eqs. (8) yields the displacements and electric potential in terms of eight arbitrary constants and the angular frequency ω. The stresses and electric displacements are obtained from Eqs. (16), (11) and (9).

The satisfaction of the homogeneous boundary conditions at the top surface and interfaces between adjoining laminae and bottom surface results in the following homogeneous matrix equation:

$$\mathbf{G}(\omega)\mathbf{W} = \mathbf{0}, \tag{17}$$

where $\mathbf{G}(\omega)$ is an $8N \times 8N$ matrix whose elements are polynomials of ω and $\mathbf{W}$ is a vector of length $8N$ consisting of the unknown constants. A nontrivial solution for $\mathbf{W}$ is obtained by setting the determinant $|\mathbf{G}(\omega)|$ equal to zero. The resulting polynomial equation is solved to obtain a set of eigenvalues that are arranged in ascending order as $\{\omega_k^{(1)}, \omega_k^{(2)}, \omega_k^{(3)}, \ldots\}$, which are the natural frequencies (eigenvalues) of the plate corresponding to the longitudinal mode shape defined by integer k. The eigenvector $\mathbf{W}^{(j)}$ associated with the eigenvalue $\omega_k^{(j)}$ is determined from the nullspace

of $\mathbf{G}(\omega_k^{(j)})$. The displacements, electric potential, stresses and electric displacement at any point within the laminate are determined using the $8N$ constants from the eigenvector $\mathbf{W}^{(j)}$.

3.2. Forced vibration analysis

The forced vibration analysis will focus on the steady-state response of the composite plate due to harmonic distributed normal loads or electric potential on the top and/or bottom surfaces as stated in Eq. (5). It should be noted that a harmonic electric potential can also be applied to the electroded interfaces as in Eq. (7). For the case of forced vibration, k and ω are known from the prescribed harmonic loads. The recurrence relations (12) are evaluated successively for $\beta = 0, 1, 2, \ldots$, to obtain $\tilde{U}_1^{(n,\beta+2)}$, $\tilde{U}_2^{(n,\beta+2)}$, $\tilde{U}_3^{(n,\beta+2)}$ and $\tilde{\Phi}^{(n,\beta+2)}$ in terms of eight arbitrary constants $\tilde{U}_1^{(n,0)}$, $\tilde{U}_2^{(n,0)}$, $\tilde{U}_3^{(n,0)}$, $\tilde{\Phi}^{(n,0)}$, $\tilde{U}_1^{(n,1)}$, $\tilde{U}_2^{(n,1)}$, $\tilde{U}_3^{(n,1)}$and $\tilde{\Phi}^{(n,1)}$ as

$$\begin{aligned}
\tilde{U}_i^{(n,\beta+2)} &= \sum_{j=1}^{3}\left[a_{ij}^{(n,\beta+2)}\tilde{U}_j^{(n,0)} + \hat{a}_{ij}^{(n,\beta+2)}\tilde{U}_j^{(n,1)}\right] + b_i^{(n,\beta+2)}\tilde{\Phi}^{(n,0)} + \hat{b}_i^{(n,\beta+2)}\tilde{\Phi}^{(n,1)},\\
\tilde{\Phi}^{(n,\beta+2)} &= \sum_{j=1}^{3}\left[q_j^{(n,\beta+2)}\tilde{U}_j^{(n,0)} + \hat{q}_j^{(n,\beta+2)}\tilde{U}_j^{(n,1)}\right] + r^{(n,\beta+2)}\tilde{\Phi}^{(n,0)} + \hat{r}^{(n,\beta+2)}\tilde{\Phi}^{(n,1)}.
\end{aligned} \tag{18}$$

Here $a_{ij}^{(n,\beta+2)}$, $\hat{a}_{ij}^{(n,\beta+2)}$, $b_i^{(n,\beta+2)}$, $\hat{b}_i^{(n,\beta+2)}$, $q_j^{(n,\beta+2)}$, $\hat{q}_j^{(n,\beta+2)}$, $r^{(n,\beta+2)}$ and $\hat{r}^{(n,\beta+2)}$ are known constants. The boundary conditions on the top and bottom surfaces of the plate, and the $N-1$ interfaces between adjoining laminae, result in the following linear system of equations for the $8N$ unknown constants:

$$\mathbf{GW} = \mathbf{Y}, \tag{19}$$

where the matrix $\mathbf{G}$ and vector $\mathbf{Y}$ are known, and $\mathbf{W}$ is a vector consisting of the $8N$ unknown constants. The linear system of equations (19) are solved to obtain the constants for each layer.

4. Active damping using feedback control

In this section, we implement active damping through feedback control. The top surface of the composite plate is subjected to the harmonic distributed load

$$\sigma_{33}^{(N)}(x_1, H/2, t) = q_0\, \mathrm{e}^{\mathrm{i}\omega t} \sin \pi x_1/L, \tag{20}$$

where the circular frequency ω is prescribed. We use two different feedback control algorithms to achieve active damping. The first is the Positive Position Feedback (PPF) controller, which was introduced by Goh and Caughey [38]. PPF control introduces a second-order compensator which is forced by the displacement response of the structure,

$$\ddot{\eta} + 2\zeta_c\omega_c\dot{\eta} + \omega_c^2\eta = \omega_c^2 u_3(L/2, H/2, t), \tag{21}$$

where η is the controller coordinate, ω_c is the natural frequency of the controller and ζ_c is the damping ratio of the controller. For steady-state vibration, the controller coordinate is also

harmonic $\eta = \eta_0 e^{i\omega t}$ and Eq. (21) becomes

$$-\omega^2\eta_0 + 2i\zeta_c\omega_c\omega\eta_0 + \omega_c^2\eta_0 = \omega_c^2 U_3^{(N)}(H/2). \tag{22}$$

The amplitude of the controller coordinate obtained from Eq. (22) is

$$\eta_0 = \left[\frac{\omega_c^2}{(\omega_c^2 - \omega^2) + 2i\zeta_c\omega_c\omega}\right] U_3^{(N)}(H/2). \tag{23}$$

The controller coordinate η, magnified by a positive gain, is then fed back as a voltage input ϕ to a piezoelectric shear actuator

$$\begin{aligned}\phi(x_1, t) &= g_p\omega_c^2\eta\cos\pi x_1/L \\ &= \left[\frac{g_p\,\omega_c^4\,U_3^{(N)}(H/2)}{(\omega_c^2 - \omega^2) + 2i\zeta_c\omega_c\omega}\right] e^{i\omega t}\cos\pi x_1/L,\end{aligned} \tag{24}$$

where g_p is the PPF gain parameter which has units of Vs^2/m.

The second controller implemented is the velocity feedback controller. The velocity feedback controller is also a second-order compensator which is forced by the velocity response of the structure

$$\ddot{\eta} + 2\zeta_c\omega_c\dot{\eta} + \omega_c^2\eta = \omega_c^2\dot{u}_3(L/2, H/2, t). \tag{25}$$

For steady-state vibration, the amplitude of the controller coordinate is harmonic $\eta = \eta_0 e^{i\omega t}$ and

$$\eta_0 = \left[\frac{i\omega\omega_c^2}{(\omega_c^2 - \omega^2) + 2i\zeta_c\omega_c\omega}\right] U_3^{(N)}(H/2). \tag{26}$$

The negative of the controller coordinate, magnified by a negative gain, is then fed back as a voltage input ϕ to a piezoelectric shear actuator:

$$\begin{aligned}\phi(x_1, t) &= -g_v\omega_c^2\eta\cos\pi x_1/L \\ &= \left[\frac{-g_v\,i\omega\,\omega_c^4\,U_3^{(N)}(H/2)}{(\omega_c^2 - \omega^2) + 2i\zeta_c\omega_c\omega}\right] e^{i\omega t}\cos\pi x_1/L,\end{aligned} \tag{27}$$

where g_v is the velocity feedback gain parameter which has units of Vs^3/m. The feedback potential of the PPF controller (24) and velocity feedback controller (27) are applied as boundary conditions to the piezoelectric shear actuator. The implementation of the other boundary conditions on the top and bottom surfaces of the laminate and the interface conditions is similar to that of forced vibration analysis discussed earlier. Since $\phi(x_1, t)$ and $U_3^{(N)}(H/2)$ are functions of the unknown constants $\tilde{U}_1^{(n,0)}$, $\tilde{U}_2^{(n,0)}$, $\tilde{U}_3^{(n,0)}$, $\tilde{\Phi}^{(n,0)}$, $\tilde{U}_1^{(n,1)}$, $\tilde{U}_2^{(n,1)}$, $\tilde{U}_3^{(n,1)}$ and $\tilde{\Phi}^{(n,1)}$, the controller parameters, ω_c, ζ_c and g_p or g_v appear on the left-hand side matrix $\mathbf{G}$ in Eq. (19). The displacements and stresses are complex valued since the feedback potential (24)/(27) is complex. The magnitude and phase of the displacements and stresses with respect to the applied harmonic load can be inferred from their respective real and imaginary parts.

5. Results and discussion

We present results for hybrid laminates with each lamina made of either fiber-reinforced graphite-epoxy or PZT-5A. The graphite-epoxy is assumed to be orthotropic with its principal material direction inclined at an angle ψ to the x_1-axis in the x_1–x_2 plane. The PZT-5A is assumed to be transversely isotropic with the x_1-axis as the axis of transverse isotropy, which is also the poling direction. The material properties of the axially poled PZT-5A were obtained by a tensor transformation of the material properties given by Tang et al. [45] of PZT-5A poled in the x_3-direction. The nonzero values of the material properties are listed in Table 1 for the PZT-5A and graphite-epoxy for $\psi = 0^\circ$ and $\pm 45^\circ$. In our analysis, we consider all the layers to be piezoelectric with the piezoelectric moduli of graphite-epoxy set equal to zero.

5.1. Natural frequencies and mode shapes

We consider a hybrid laminate with the top and bottom layers made of 0° graphite-epoxy and the central layer made of axially poled PZT-5A, i.e. a [0° Gr-Ep/PZT-5A/0° Gr-Ep] laminate. The thickness of the graphite-epoxy layers is $0.4H$, the thickness of the PZT-5A layer is $0.2H$. The location of the bottom surface, the interfaces between laminae and top surface of the hybrid

Table 1
Nonvanishing material properties of graphite-epoxy and PZT-5A shear actuators

Property	0° graphite-epoxy	$\pm 45^\circ$ graphite-epoxy	PZT-5A
C_{11} (GPa)	183.443	58.128	86.856
C_{22} (GPa)	11.662	58.128	99.201
C_{33} (GPa)	11.662	11.662	99.201
C_{12} (GPa)	4.363	43.788	50.778
C_{13} (GPa)	4.363	4.140	50.778
C_{23} (GPa)	3.918	4.140	54.016
C_{44} (GPa)	2.870	5.020	22.600
C_{55} (GPa)	7.170	5.020	21.100
C_{66} (GPa)	7.170	46.595	21.100
C_{16} (GPa)	0	± 42.945	0
C_{26} (GPa)	0	± 42.945	0
C_{36} (GPa)	0	± 0.222	0
C_{45} (GPa)	0	± 2.150	0
e_{11} (Cm^{-2})	0	0	15.118
e_{12} (Cm^{-2})	0	0	-7.209
e_{13} (Cm^{-2})	0	0	-7.209
e_{26} (Cm^{-2})	0	0	12.322
e_{35} (Cm^{-2})	0	0	12.322
ϵ_{11} (10^{-10} F/m)	153.0	153.0	150.0
ϵ_{22} (10^{-10} F/m)	153.0	153.0	153.0
ϵ_{33} (10^{-10} F/m)	153.0	153.0	153.0
ρ ($\mathrm{kg/m}^3$)	1590	1590	7750

laminate are $H^{(1)} = -0.5H$, $H^{(2)} = -0.1H$, $H^{(3)} = 0.1H$ and $H^{(4)} = 0.5H$. The interfaces between the PZT-5A lamina and the graphite-epoxy laminae at $x_3 = H^{(2)}$ and $x_3 = H^{(3)}$ are perfectly bonded. The top and bottom surfaces of the PZT-5A laminae are assumed to be either

(1) *electrically closed*: $\phi^{(1)}(x_1, -0.1H, t) = \phi^{(2)}(x_1, -0.1H, t) = 0$, $\phi^{(2)}(x_1, 0.1H, t) = \phi^{(3)}(x_1, 0.1H, t) = 0$, or

(2) *electrically open*: $\phi^{(1)}(x_1, -0.1H, t) = \phi^{(2)}(x_1, -0.1H, t)$, $D_3^{(1)}(x_1, -0.1H, t) = D_3^{(2)}(x_1, -0.1H, t)$, $\phi^{(2)}(x_1, 0.1H, t) = \phi^{(3)}(x_1, 0.1H, t)$, $D_3^{(2)}(x_1, 0.1H, t) = D_3^{(3)}(x_1, 0.1H, t)$.

The top and bottom surfaces of the laminate are electrically insulated ($D_3^{(1)}(x_1, -H/2, t) = D_3^{(3)}(x_1, H/2, t) = 0$). The length L is chosen to be 0.25 m. We consider three different length-to-thickness (L/H) ratios of 4, 10 and 100, which characterize a thick, moderately thick and thin laminate, respectively. Thirty five terms in the series solution (11) are used to obtain results that are accurate to six significant digits. The natural frequencies are computed for different values of k and arranged in ascending order.

The first 12 natural frequencies for the hybrid plate are listed in Table 2 for electrically closed and open boundary conditions. In addition, a plane strain numerical solution was computed using the commercial finite element program ABAQUS/Standard 6.3-1 [46] with 15,700 8-node biquadratic elements to ensure that there was no algebraic errors in the implementation of the exact solution. The finite-element natural frequencies are listed in parenthesis next to the exact results in Table 2. It shows good agreement between the exact and finite-element solutions. Since ABAQUS does not have a generalized plane strain element for piezoelectric materials, the out-of-plane modes with displacement in the x_2-direction cannot be captured by the plane strain finite-element solution and are indicated by (- -) in Table 2. For $L/H = 4$, six out of the lowest 12 modes are out-of-plane modes that have nonzero displacement in the x_2-direction. However, for $L/H = 100$, only three of the modes are out-of-plane modes. The analytically obtained mode shapes for $L/H = 4$ and electrically closed boundary conditions are depicted in Fig. 2 by plotting the deformed shapes of material lines that in the reference configuration are parallel to the coordinate axes. Although the plate is assumed to be of infinite width in the x_2-direction, the mode shapes are truncated to a finite width for the purpose of illustration. The higher modes of vibration are more sensitive to the electrical boundary conditions on the top and bottom surfaces of the piezoelectric layer than the lower modes. For example, for $L/H = 4$, the thickness mode natural frequency $\omega_1^{(3)}$ changes by 321.1 Hz depending on whether it is electrically closed or open. In comparison, the fundamental frequency $\omega_1^{(1)}$ changes only by 33.8 Hz. For a thick laminate with $L/H = 4$, only five of the lowest 12 natural frequencies, namely $\omega_k^{(1)}$ with $k = 1, \ldots, 5$ correspond to flexural modes. In contrast, a thin laminate with $L/H = 100$ has nine flexural modes $\omega_k^{(1)}$ in the lowest 12 natural frequencies, namely $k = 1, \ldots, 9$. It should also be noted that the natural frequencies of the out-of-plane modes remain essentially constant for all length-to-thickness ratios. For example, the natural frequency $\omega_1^{(2)} = 3752.27$, 3755.9 and 3756.58 Hz for $L/H = 4$, 10 and 100, respectively.

Next, we consider a three-layer [45° Gr-Ep/PZT-5A/−45° Gr-Ep] hybrid laminate that is unsymmetric about the midsurface. Except for the orientation of the principal material directions of the graphite-epoxy layers, the geometry and dimensions remain the same as the [0° Gr-Ep/PZT-5A/0° Gr-Ep] laminate discussed earlier. The off-axis graphite-epoxy layers introduce strong

Table 2
First 12 natural frequencies of a [0° Gr-Ep/PZT-5A/0° Gr-Ep] hybrid laminate for $L = 0.25$ m and $L/H = 4$, 10 and 100

$L/H = 4$				$L/H = 10$				$L/H = 100$			
Mode	Closed (Hz)	Mode	Open (Hz)	Mode	Closed (Hz)	Mode	Open (Hz)	Mode	Closed (Hz)	Mode	Open (Hz)
$\omega_1^{(1)}$	2449.9 (2449.9)	$\omega_1^{(1)}$	2483.73 (2483.7)	$\omega_1^{(1)}$	1328.91 (1328.9)	$\omega_1^{(1)}$	1334.23 (1334.2)	$\omega_1^{(1)}$	145.057 (145.06)	$\omega_1^{(1)}$	145.064 (145.06)
$\omega_1^{(2)}$	3752.27 (–)	$\omega_1^{(2)}$	3752.27 (–)	$\omega_1^{(2)}$	3755.9 (–)	$\omega_1^{(2)}$	3755.9 (–)	$\omega_2^{(1)}$	578.545 (578.55)	$\omega_2^{(1)}$	578.655 (578.66)
$\omega_2^{(1)}$	6085.51 (6085.5)	$\omega_2^{(1)}$	6219.85 (6219.9)	$\omega_2^{(1)}$	4367.51 (4367.5)	$\omega_2^{(1)}$	4415.16 (4415.2)	$\omega_3^{(1)}$	1295.49 (1295.5)	$\omega_3^{(1)}$	1296.04 (1296.0)
$\omega_2^{(2)}$	7479.11 (–)	$\omega_2^{(2)}$	7479.11 (–)	$\omega_2^{(2)}$	7507.64 (–)	$\omega_2^{(2)}$	7507.64 (–)	$\omega_4^{(1)}$	2287.84 (2287.8)	$\omega_4^{(1)}$	2289.53 (2289.5)
$\omega_3^{(1)}$	9678.38 (9678.4)	$\omega_3^{(1)}$	9931.1 (9931.1)	$\omega_3^{(1)}$	7931.9 (7931.9)	$\omega_3^{(1)}$	8060.28 (8060.3)	$\omega_5^{(1)}$	3544.82 (3544.8)	$\omega_5^{(1)}$	3548.85 (3548.8)
$\omega_3^{(2)}$	11158.1 (–)	$\omega_3^{(2)}$	11158.1 (–)	$\omega_3^{(2)}$	11251.1 (–)	$\omega_3^{(2)}$	11251.1 (–)	$\omega_1^{(2)}$	3756.58 (–)	$\omega_1^{(2)}$	3756.58 (–)
$\omega_4^{(1)}$	13238.5 (13239)	$\omega_4^{(1)}$	13625.6 (13626)	$\omega_4^{(1)}$	11580.3 (11580)	$\omega_4^{(1)}$	11808.1 (11808)	$\omega_6^{(1)}$	5053.35 (5053.3)	$\omega_6^{(1)}$	5061.46 (5061.5)
$\omega_1^{(3)}$	13368.6 (13369)	$\omega_1^{(4)}$	13684.7 (–)	$\omega_1^{(3)}$	14674.1 (14674)	$\omega_1^{(3)}$	14907.4 (14907)	$\omega_7^{(1)}$	6798.55 (6798.6)	$\omega_7^{(1)}$	6813.07 (6813.1)
$\omega_1^{(4)}$	13684.7 (–)	$\omega_1^{(3)}$	13689.7 (13689)	$\omega_4^{(2)}$	14982.4 (–)	$\omega_4^{(2)}$	14982.4 (–)	$\omega_2^{(2)}$	7513.13 (–)	$\omega_2^{(2)}$	7513.13 (–)
$\omega_4^{(2)}$	14773.4 (–)	$\omega_4^{(2)}$	14773.4 (–)	$\omega_5^{(1)}$	15213.8 (15214)	$\omega_5^{(1)}$	15549.6 (15550)	$\omega_8^{(1)}$	8764.26 (8764.3)	$\omega_8^{(1)}$	8788.09 (8788.1)
$\omega_5^{(1)}$	16777.4 (16777)	$\omega_1^{(5)}$	17156 (–)	$\omega_5^{(2)}$	18697.8 (–)	$\omega_5^{(2)}$	18697.8 (–)	$\omega_9^{(1)}$	10933.5 (10934)	$\omega_9^{(1)}$	10970.1 (10970)
$\omega_1^{(5)}$	17156 (–)	$\omega_5^{(1)}$	17315.3 (17315)	$\omega_6^{(1)}$	18821.2 (18821)	$\omega_6^{(1)}$	19271 (19271)	$\omega_3^{(2)}$	11269.6 (–)	$\omega_3^{(2)}$	11269.6 (–)

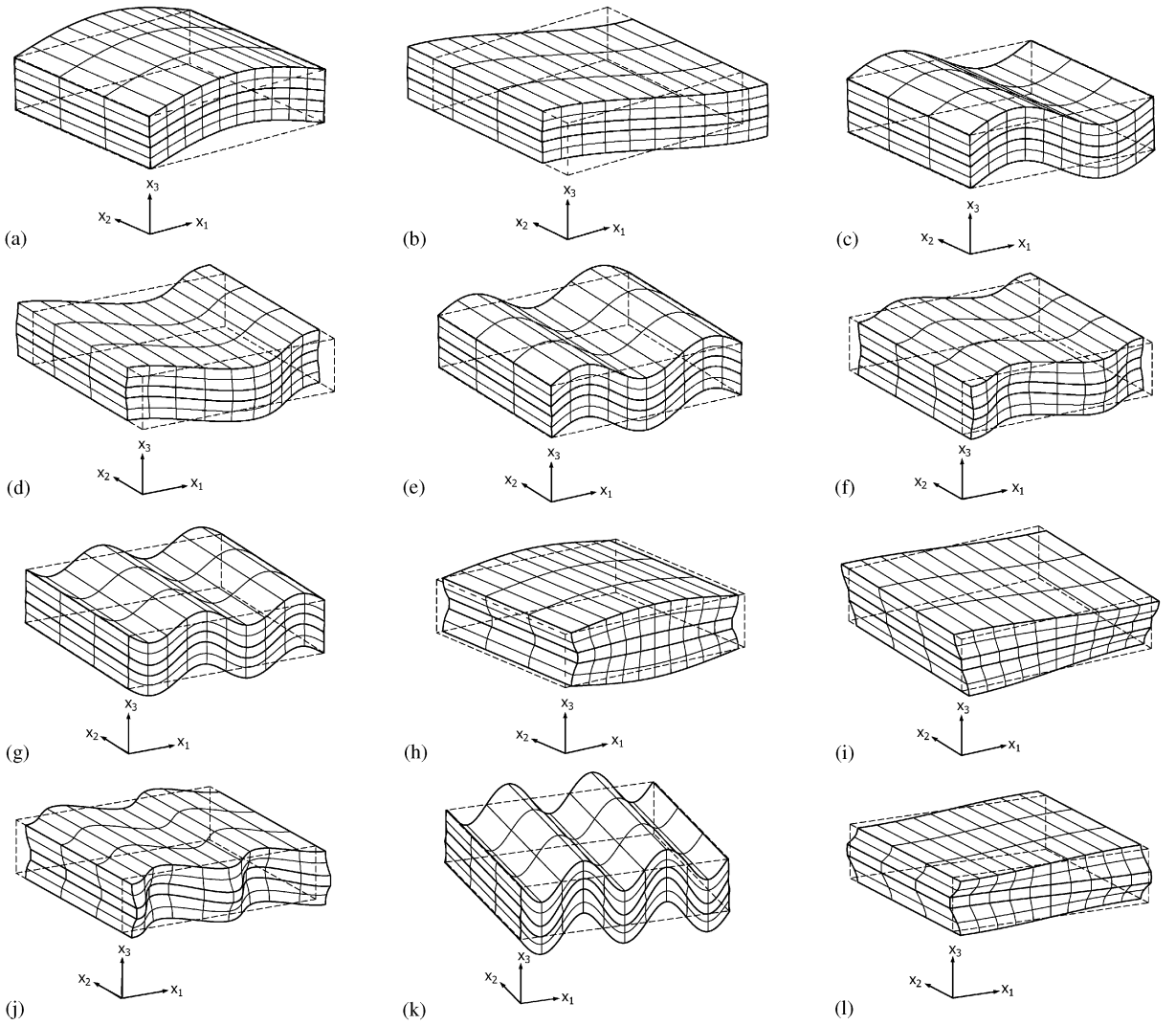

Fig. 2. First 12 mode shapes and natural frequencies for a [0° Gr-Ep/PZT-5A/0° Gr-Ep] hybrid laminate, electrically closed, $L = 0.25$ m, $L/H = 4$: (a) $\omega_1^{(1)} = 2449.9$ Hz, (b) $\omega_1^{(2)} = 3752.27$ Hz, (c) $\omega_2^{(1)} = 6085.51$ Hz, (d) $\omega_2^{(2)} = 7479.11$ Hz, (e) $\omega_3^{(1)} = 9678.38$ Hz, (f) $\omega_3^{(2)} = 11158.1$ Hz, (g) $\omega_4^{(1)} = 13238.5$ Hz, (h) $\omega_1^{(3)} = 13368.6$ Hz, (i) $\omega_1^{(4)} = 13684.76$ Hz, (j) $\omega_4^{(2)} = 14773.4$ Hz, (k) $\omega_5^{(1)} = 16777.4$ Hz, (l) $\omega_1^{(5)} = 17156$ Hz.

coupling of the displacement components u_1 and u_3 to the out-of-plane displacement component u_2. The lowest 12 natural frequencies for a thick plate with $L/H = 4$ is given in Table 3 for electrically closed and open boundary conditions. The mode shapes corresponding to the closed boundary conditions are depicted in Fig. 3. The effect of the strong coupling is very evident in the figure. For example, the mode shapes shown in Figs. 3(e) and (i) are primarily a combination of thickness distention and shear in the x_2–x_3 plane. Through-the-thickness plots of the displacements and electric potential corresponding to the lowest nine natural frequencies are

Table 3
First 12 natural frequencies of a [45° Gr-Ep/PZT-5A/−45° Gr-Ep] hybrid laminate for $L = 0.25$ m and $L/H = 4$

$L/H = 4$			
Mode	Closed (Hz)	Mode	Open (Hz)
$\omega_1^{(1)}$	1210.29	$\omega_1^{(1)}$	1212.93
$\omega_2^{(1)}$	3786.37	$\omega_2^{(1)}$	3805.64
$\omega_3^{(1)}$	6721.76	$\omega_3^{(1)}$	6770.05
$\omega_1^{(2)}$	6936.61	$\omega_1^{(2)}$	6971.56
$\omega_1^{(3)}$	8186.22	$\omega_1^{(3)}$	8559.04
$\omega_4^{(1)}$	9733.10	$\omega_4^{(1)}$	9818.43
$\omega_2^{(2)}$	11881.4	$\omega_2^{(2)}$	12003.6
$\omega_5^{(1)}$	12758.8	$\omega_5^{(1)}$	12886.8
$\omega_2^{(3)}$	13631.9	$\omega_2^{(3)}$	14171.2
$\omega_1^{(4)}$	15583.7	$\omega_1^{(4)}$	15661.4
$\omega_6^{(1)}$	15788.9	$\omega_6^{(1)}$	15963.9
$\omega_1^{(5)}$	15893.9	$\omega_1^{(5)}$	15955.2

shown in Figs. 4(a)–(i) at specific axial locations. The variables are plotted after normalization by their respective maximum values. The axial displacement u_1 has essentially a linear variation in the thickness direction for the fundamental frequency shown in Fig. 4(a), as is usually assumed in the classical plate theory. However, u_1 is highly nonlinear for the higher modes as evident in Fig. 4(h). The potential in the piezoelectric layer has an approximately parabolic or *S*-shaped cubic variation. The through-the-thickness variation of the stress components σ_{11}, σ_{12}, σ_{33} and σ_{13} corresponding to the first nine modes are presented in Fig. 5. The longitudinal stress σ_{11} is essentially linear in the thickness direction within each lamina for the fundamental frequency $\omega_1^{(1)}$. For the higher modes, the longitudinal stress σ_{11} has a nonlinear variation in the graphite-epoxy layers and an essentially linear variation in the piezoelectric layer. The shear stress σ_{12} and longitudinal stress σ_{11} are discontinuous at the interfaces between the graphite-epoxy and piezoelectric laminae due to the abrupt change in material properties. The transverse shear stress σ_{13} has an approximately parabolic variation through the thickness for the flexural modes shown in Figs. 5(a)–(c), (f) and (h).

5.2. Active damping

Consider the [0° Gr-Ep/PZT-5A/0° Gr-Ep] hybrid laminate discussed in the previous section of length $L = 0.25$ m and $L/H = 10$. It is subjected to the harmonic distributed load (20) on the top surface. We employ a PPF controller to achieve active damping. A second-order PPF compensator is forced by the transverse displacement of the midpoint of the top surface and the feedback voltage (24) is applied to the top surface of the PZT-5A shear actuator at $x_3 = 0.1H$. The bottom surface of the piezoelectric actuator at $x_3 = -0.1H$ is electrically grounded. It is assumed that the graphite-epoxy and piezoelectric laminae do not exhibit material damping.

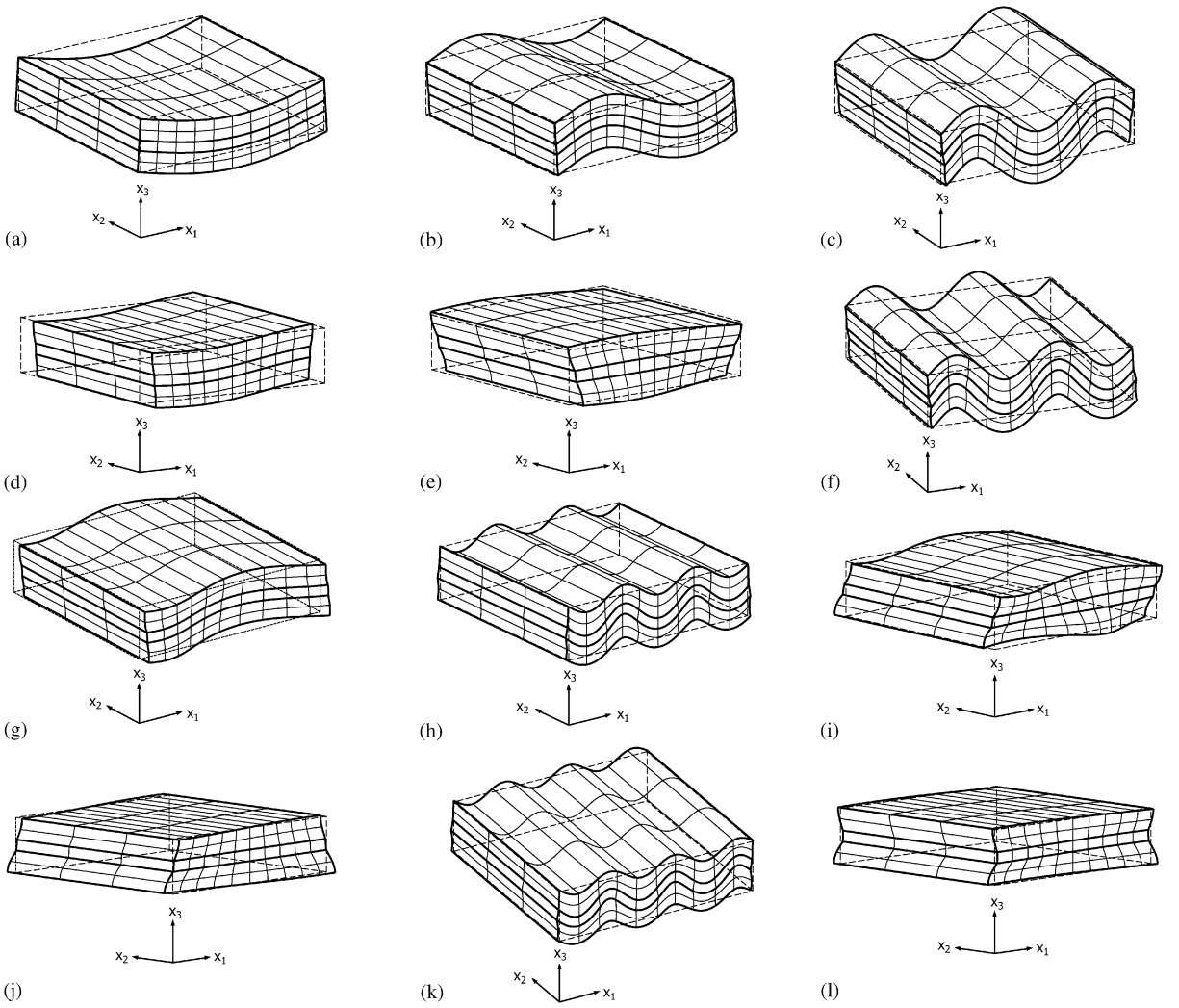

Fig. 3. First 12 mode shapes and natural frequencies for a [45° Gr-Ep/PZT-5A/−45° Gr-Ep] hybrid laminate, electrically closed, $L = 0.25\,\text{m}$, $L/H = 4$: (a) $\omega_1^{(1)} = 1210.29\,\text{Hz}$, (b) $\omega_2^{(1)} = 3786.37\,\text{Hz}$, (c) $\omega_3^{(1)} = 6721.76\,\text{Hz}$, (d) $\omega_1^{(2)} = 6936.61\,\text{Hz}$, (e) $\omega_1^{(3)} = 8186.22\,\text{Hz}$, (f) $\omega_4^{(1)} = 9733.10\,\text{Hz}$, (g) $\omega_2^{(2)} = 11881.4\,\text{Hz}$, (h) $\omega_5^{(1)} = 12758.8\,\text{Hz}$, (i) $\omega_2^{(3)} = 13631.9\,\text{Hz}$, (j) $\omega_1^{(4)} = 15583.7\,\text{Hz}$, (k) $\omega_6^{(1)} = 15788.9\,\text{Hz}$, (l) $\omega_1^{(5)} = 15893.9\,\text{Hz}$.

Therefore, any damping of the hybrid laminated plate is a result of the PPF controller. We seek to quantify the effectiveness of the piezoelectric shear actuator and the PPF controller for vibration suppression. For a given choice of control parameters ω_c, ζ_c and g, the steady-state response of the system is computed for a given forcing frequency ω. The magnitude and phase of the transverse deflection is plotted as function of the forcing frequency ω for different controller parameters to obtain frequency-response curves.

Targeted vibration suppression of the fundamental mode of vibration is achieved by choosing the compensator frequency ω_c to be approximately equal to the fundamental frequency

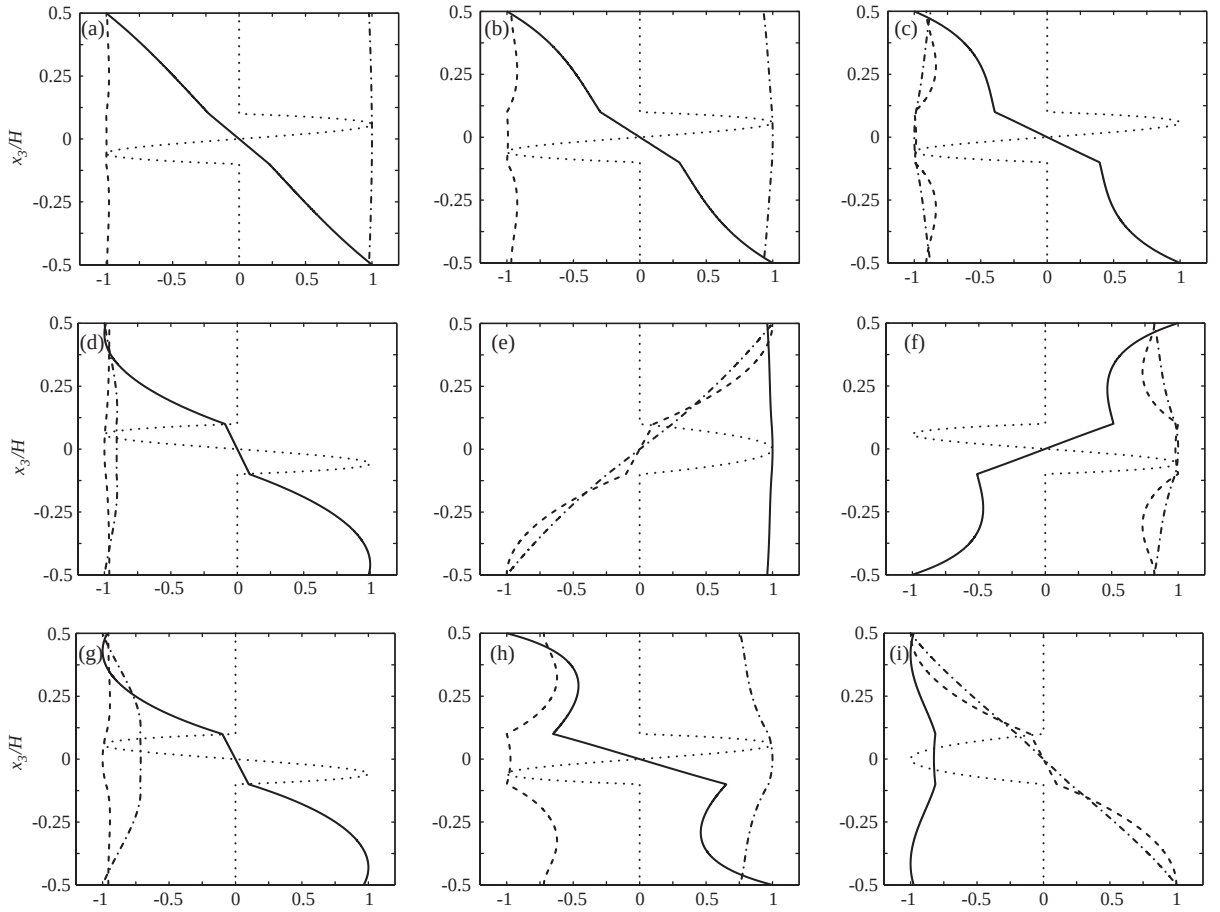

Fig. 4. The first nine through-the-thickness displacement and stress mode shapes for a [45° Gr-Ep/PZT-5A/−45° Gr-Ep] hybrid laminate, $L = 0.25\,\text{m}$, $L/H = 4$: ——, $u_1(0,x_3)/\text{Max}|u_1(0,x_3)|$; – – –, $u_2(0,x_3)/\text{Max}|u_2(0,x_3)|$; –.–.–, $u_3(L/2,x_3)/\text{Max}|u_3(L/2,x_3)|$; ⋯⋯, $\phi(0,x_3)/\text{Max}|\phi(0,x_3)|$. (a) $\omega_1^{(1)} = 1210.29\,\text{Hz}$, (b) $\omega_2^{(1)} = 3786.37\,\text{Hz}$, (c) $\omega_3^{(1)} = 6721.76\,\text{Hz}$, (d) $\omega_1^{(2)} = 6936.61\,\text{Hz}$, (e) $\omega_1^{(3)} = 8186.22\,\text{Hz}$, (f) $\omega_4^{(1)} = 9733.10\,\text{Hz}$, (g) $\omega_2^{(2)} = 11881.4\,\text{Hz}$, (h) $\omega_5^{(1)} = 12758.8\,\text{Hz}$, (i) $\omega_2^{(3)} = 13631.9\,\text{Hz}$.

$\omega_1^{(1)} = 1328.91\,\text{Hz}$ (Table 2). Fig. 6(a) shows the frequency response curves for controller frequencies of $\omega_c = \omega_1^{(1)}$, $1.1\omega_1^{(1)}, 1.35\omega_1^{(1)}$ and $1.4\omega_1^{(1)}$. The controller parameters ζ_c and g_p were kept constant at 0.05 and $0.1\,\text{Vs}^2/\text{m}$, respectively, for results in Fig. 6(a). The magnitude of the transverse deflection is normalized by the forcing function amplitude q_0, L and C_0, which have values of $1\,\text{N/m}^2$, 0.25 m and 21.1 GPa, respectively. It is observed that the maximum system damping is achieved when the controller frequency ω_c is chosen to be equal to the fundamental frequency $\omega_1^{(1)}$. The corresponding phase difference between the transverse deflection and the applied harmonic load is shown in Fig. 6(b) as function of the forcing frequency ω. The magnitude and phase frequency response curves for controller damping ratios $\zeta_c = 0.05, 0.15, 0.35$ and 0.5 are shown in Fig. 6(c) and (d) for controller frequency $\omega_c = \omega_1^{(1)}$ and $g_p = 0.1\,\text{Vs}^2/\text{m}$. The figure shows a decrease in system damping for increasing controller damping ratio. The response

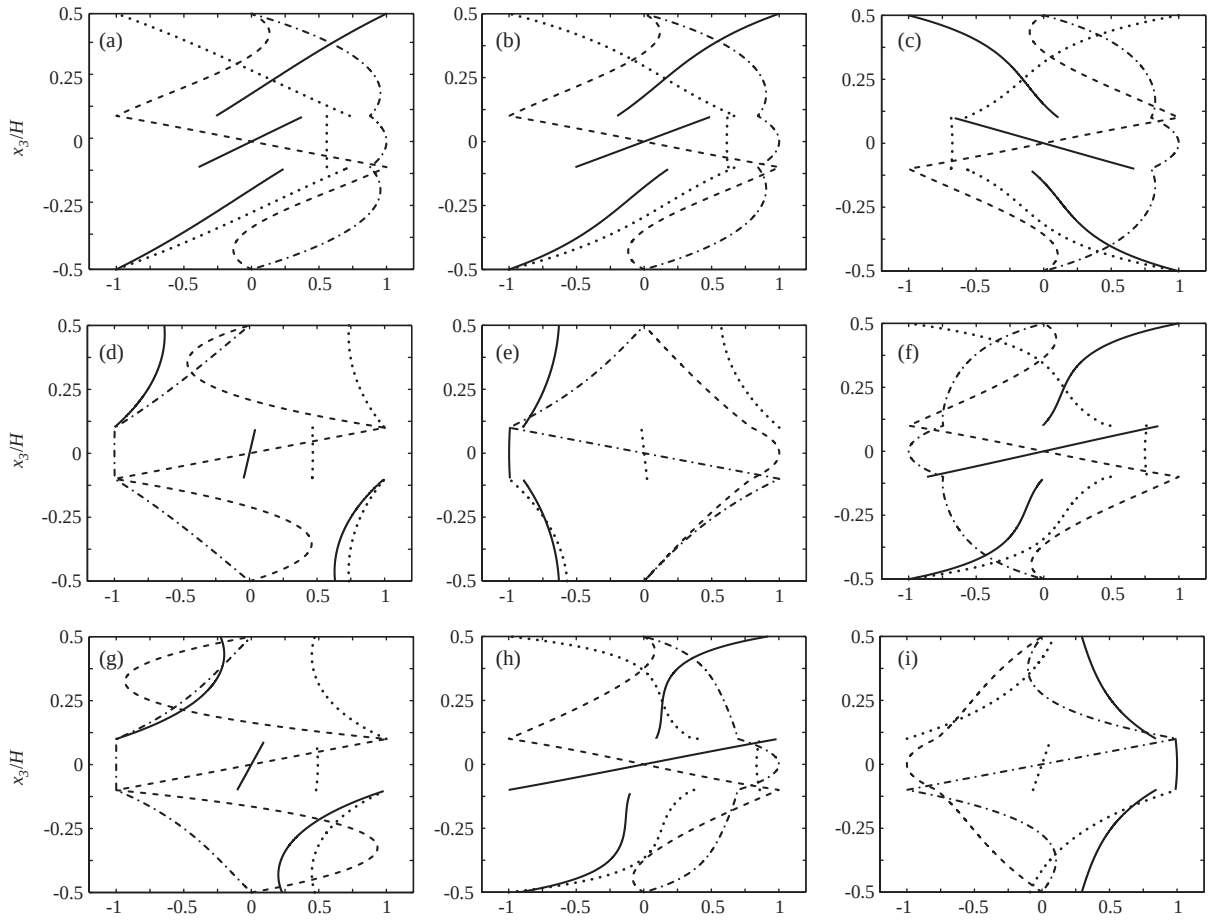

Fig. 5. The first nine through-the-thickness displacement and stress mode shapes for a [45° Gr-Ep/PZT-5A/−45° Gr-Ep] hybrid laminate, $L = 0.25$ m, $L/H = 4$: ——, $\sigma_{11}(L/2, x_3)/\text{Max}|\sigma_{11}(L/2, x_3)|$; – – –, $\sigma_{33}(L/2, x_3)/\text{Max}|\sigma_{33}(L/2, x_3)|$; –.–.–, $\sigma_{13}(0, x_3)\text{Max}|\sigma_{13}(0, x_3)|$; ⋯⋯, $\sigma_{12}(L/2, x_3)/\text{Max}|\sigma_{12}(L/2, x_3)|$. (a) $\omega_1^{(1)} = 1210.29$ Hz, (b) $\omega_2^{(1)} = 3786.37$ Hz, (c) $\omega_3^{(1)} = 6721.76$ Hz, (d) $\omega_1^{(2)} = 6936.61$ Hz, (e) $\omega_1^{(3)} = 8186.22$ Hz, (f) $\omega_4^{(1)} = 9733.10$ Hz, (g) $\omega_2^{(2)} = 11881.4$ Hz, (h) $\omega_5^{(1)} = 12758.8$ Hz, (i) $\omega_2^{(3)} = 13631.9$ Hz.

of the system due to changes in the PPF gain parameter g_p is evident from Fig. 6(e). As the parameter g_p is increased, the system damping also increases. For large values of g_p, the magnitude of transverse deflection at the system's fundamental frequency $\omega = 1328.91$ Hz is *smaller* than at $\omega = 1000$ or 1500 Hz. This is a result of extremely targeted vibration suppression at the fundamental frequency.

The efficacy of the PPF controller for active vibration suppression of the thickness vibration mode shown in Fig. 2(h) is investigated next. The natural frequency of this thickness mode for $L/H = 10$ is $\omega_1^{(3)} = 14674.1$ Hz. The nonzero axial electric field E_1 will influence the transverse normal strain ε_{33} and the transverse normal stress σ_{33} through the piezoelectric coefficient e_{13}. Therefore, the feedback controller will introduce active damping in the thickness vibration modes that exhibit significant transverse normal strain ε_{33}. Fig. 7(a) contains the frequency response

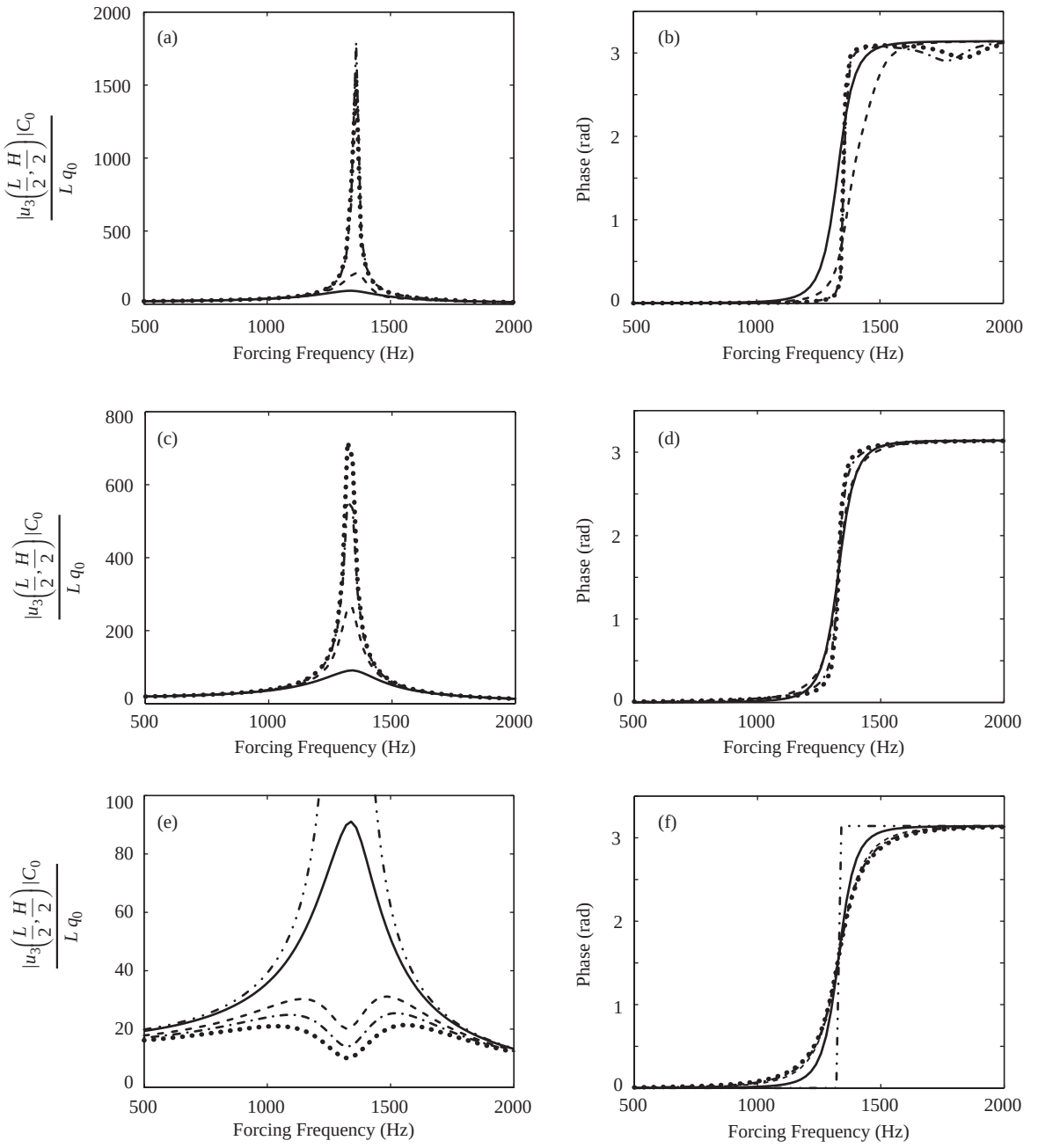

Fig. 6. Magnitude and phase frequency response curves of transverse deflection with respect to harmonic distributed load for a [0° Gr-Ep/PZT-5A/0° Gr-Ep] hybrid laminate with PPF control, $L = 0.25\,\text{m}$, $L/H = 4$: (a,b) $\zeta_c = 0.05$, $g_p = 0.1\,\text{Vs}^2/\text{m}$: ——, $\omega_c = \omega_1^{(1)}$; – – –, $\omega_c = 1.1\omega_1^{(1)}$; –.–.–, $\omega_c = 1.35\omega_1^{(1)}$; ·····, $\omega_c = 1.4\omega_1^{(1)}$, (c,d) $\omega_c = \omega_1^{(1)}$, $g_p = 0.1\,\text{Vs}^2/\text{m}$: ——, $\zeta_c = 0.05$; – – –, $\zeta_c = 0.15$; –.–.–, $\zeta_c = 0.35$; ·····, $\zeta_c = 0.5$, (e, f) $\omega_c = \omega_1^{(1)}$, $\zeta_c = 0.05$: –..–..–.., $g_p = 10^{-8}\,\text{Vs}^2/\text{m}$; ——, $g_p = 0.1\,\text{Vs}^2/\text{m}$; – – –, $g_p = 0.45\,\text{Vs}^2/\text{m}$; –.–.–, $g_p = 0.65\,\text{Vs}^2/\text{m}$; ·····, $g_p = 0.9\,\text{Vs}^2/\text{m}$.

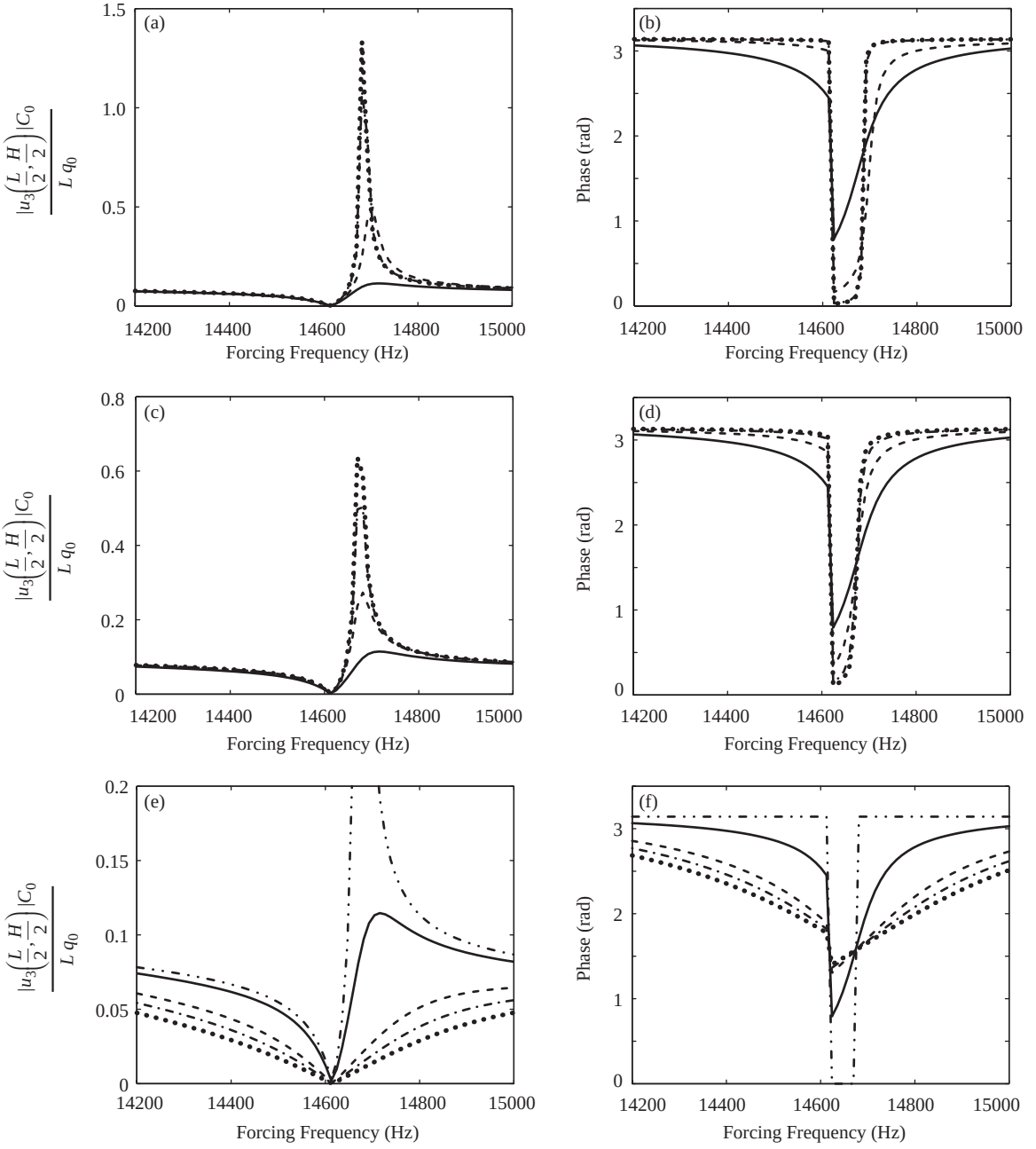

Fig. 7. Magnitude and phase frequency response curves of transverse deflection with respect to harmonic distributed load for a [0° Gr-Ep/PZT-5A/0° Gr-Ep] hybrid laminate with PPF control, $L = 0.25\,\mathrm{m}$, $L/H = 4$: (a,b) $\zeta_c = 0.05$, $g_p = 0.1\,\mathrm{Vs^2/m}$: ——, $\omega_c = \omega_1^{(3)}$; – – –, $\omega_c = 1.1\omega_1^{(3)}$; –.–.–, $\omega_c = 1.35\omega_1^{(3)}$; ……, $\omega_c = 1.4\omega_1^{(3)}$, (c,d) $\omega_c = \omega_1^{(3)}$, $g_p = 0.1\,\mathrm{Vs^2/m}$: ——, $\zeta_c = 0.05$; – – –, $\zeta_c = 0.15$; –.–.–, $\zeta_c = 0.35$; ……, $\zeta_c = 0.5$, (e,f) $\omega_c = \omega_1^{(3)}$, $\zeta_c = 0.05$: –..–..–.., $g_p = 10^{-8}\,\mathrm{Vs^2/m}$; ——, $g_p = 0.1\,\mathrm{Vs^2/m}$; – – –, $g_p = 0.45\,\mathrm{Vs^2/m}$; –.–.–, $g_p = 0.65\,\mathrm{Vs^2/m}$; ……, $g_p = 0.9\,\mathrm{Vs^2/m}$.

curves for four different controller frequencies $\omega_c = \omega_1^{(3)}$, $1.1\omega_1^{(3)}$, $1.35\omega_1^{(3)}$ and $1.4\omega_1^{(3)}$. It shows that vibration suppression of a thickness mode using a PPF controller is feasible. The largest damping is achieved when the controller frequency ω_c is equal to the natural frequency $\omega_1^{(3)}$. As expected, a phase shift occurs at the natural frequency $\omega = 14674.1$ Hz as shown in Fig. 7(b). Interestingly, the hybrid plate exhibits very small deflection and a discrete phase shift at $\omega = 14613.7$ Hz. The transverse deflection without feedback control at $\omega = 14613.7$ Hz is $|u_3(L/2, H/2)C_0/Lq_0| = 5.944 \times 10^{-3}$. As before, the frequency response curves for various controller damping ratios, depicted in Fig. 7(c) and (d), show that a smaller controller damping ratio increases the system damping. As expected, a larger gain parameter g_p increases the system damping, as shown in Figs. 7(e) and (f).

The frequency-response curves for velocity feedback control of the fundamental mode of vibration at 1328.91 Hz are depicted in Fig. 8. This shows that vibration suppression can also be achieved using a velocity feedback controller. The velocity feedback controller decreases the frequency where the maximum transverse deflection occurs. As evident from Figs. 8(a) and 6(a), the performance of the velocity feedback controller is less sensitive to the controller frequency ω_c compared to the PPF controller.

6. Conclusions

We have derived an exact solution for the cylindrical bending vibration and active damping of composite plates with embedded piezoelectric shear actuators. The edges of the composite plate are simply supported. The governing equations of linear piezoelectricity, the boundary conditions at the simply supported edges and the interface conditions between dissimilar layers are exactly satisfied. Suitable displacement and electric potential functions that identically satisfy the boundary conditions are used to reduce the equations that govern the steady-state vibrations of a hybrid plate to a set of coupled ordinary differential equations, which are then solved by employing the power series method. The exact solution thus obtained is valid for any length-to-thickness ratio.

The first 12 natural frequencies, mode shapes and through-the-thickness plots of the displacements and stresses are presented for sandwich plates consisting of axially poled piezoelectric core sandwiched between two elastic surface layers. For a thin [0° Gr-Ep/PZT-5A/0° Gr-Ep] laminate with $L/H = 100$, nine of the lowest 12 natural frequencies correspond to flexural modes of vibration. However, only five of the lowest 12 natural frequencies correspond to flexural modes for a thick laminate with $L/H = 4$. It is observed that a three-layer [45° Gr-Ep/PZT-5A/−45° Gr-Ep] hybrid laminate exhibits strong coupling of the displacement components u_1 and u_3 to the out-of-plane displacement component u_2.

Active damping is implemented using either a PPF or velocity feedback controller. PPF control introduces a second-order compensator which is forced by the transverse displacement response of the structure. The controller coordinate, magnified by a gain, is then fed back as a voltage input to a piezoelectric shear actuator. It is found that the PPF controller is effective for active damping of flexural and thickness modes of vibration. Frequency-response curves are presented for various controller frequencies, controller damping ratios and feedback gain parameters. It is found that a velocity feedback controller can also be used for vibration suppression.

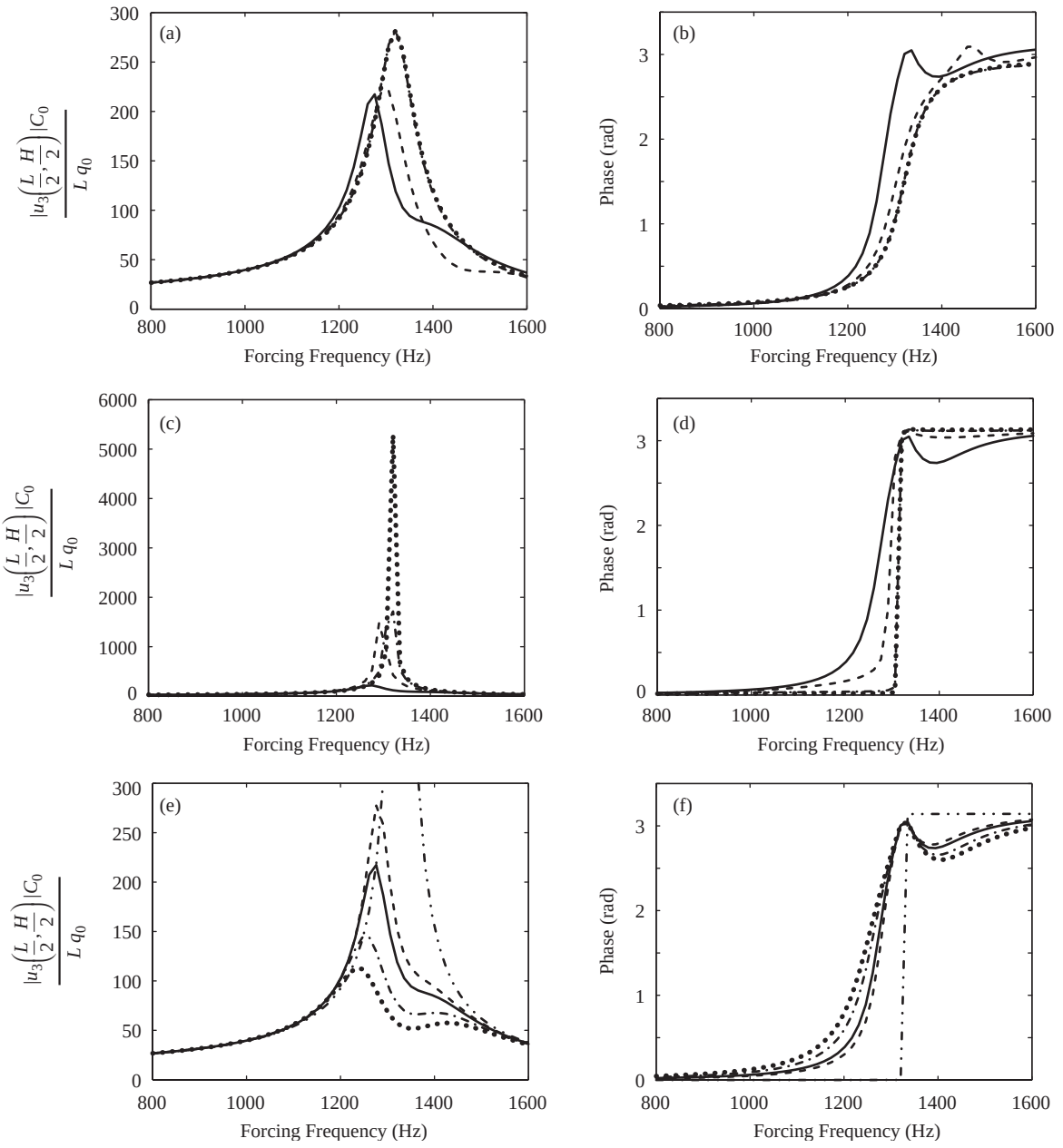

Fig. 8. Magnitude and phase frequency response curves of transverse deflection with respect to harmonic distributed load for a [0° Gr-Ep/PZT-5A/0° Gr-Ep] hybrid laminate with velocity feedback control, $L = 0.25\,\mathrm{m}$, $L/H = 4$: (a,b) $\zeta_c = 0.05$, $g_v = 1 \times 10^{-5}\ \mathrm{Vs^3/m}$: ——, $\omega_c = \omega_1^{(1)}$; – – –, $\omega_c = 1.1\omega_1^{(1)}$; –.–.–, $\omega_c = 1.35\omega_1^{(1)}$; ·····, $\omega_c = 1.4\omega_1^{(1)}$, (c,d) $\omega_c = \omega_1^{(1)}$, $g_v = 1 \times 10^{-5}\,\mathrm{Vs^3/m}$: ——, $\zeta_c = 0.05$; – – –, $\zeta_c = 0.15$; –.–.–, $\zeta_c = 0.35$; ·····, $\zeta_c = 0.5$, (e,f) $\omega_c = \omega_1^{(1)}$, $\zeta_c = 0.05$: –..–..–.., $g_v = 10^{-8}\,\mathrm{Vs^3/m}$; – – –, $g_v = 8 \times 10^{-6}\,\mathrm{Vs^3/m}$; ——, $g_v = 1 \times 10^{-5}\,\mathrm{Vs^3/m}$; –.–.–, $g_v = 1.5 \times 10^{-5}\,\mathrm{Vs^3/m}$; ·····, $g_v = 2 \times 10^{-5}\,\mathrm{Vs^3/m}$.

Acknowledgements

The authors gratefully acknowledge the support of the Maine Space Grant Consortium under collaborative seed Grant No. EP-02-11.

References

[1] C.R. Fuller, S.J. Elliott, P.A. Nelson, *Active Control of Vibration*, Academic Press, New York, 1997.
[2] T. Bailey, J.E. Hubbard Jr., Distributed piezoelectric polymer active vibration control of a cantilever beam, *AIAA Journal of Guidance, Control and Dynamics* 8 (1985) 605–611.
[3] E. Garcia, J. Dosch, D.J. Inman, The application of smart structures to the vibration suppression problem, *Journal of Intelligent Material Systems and Structures* 3 (1992) 659–667.
[4] R.L. Clark, C.R. Fuller, Experiments on active control of structurally radiated sound using multiple piezoelectric actuators, *Journal of the Acoustical Society of America* 91 (1992) 3313–3320.
[5] C.Y. Hsu, C.C. Lin, L. Gaul, Vibration and sound radiation controls of beams using layered modal sensors and actuators, *Smart Materials and Structures* 7 (1998) 446–455.
[6] D.B. Koconis, L.P. Kollar, G.S. Springer, Shape control of composite plates and shells with embedded actuators. II. Desired shape specified, *Journal of Composite Materials* 28 (1994) 459–482.
[7] B.N. Agrawal, K.E. Treanor, Shape control of a beam using piezoelectric actuators, *Smart Materials and Structures* 8 (1999) 729–740.
[8] E.F. Crawley, E.H. Anderson, Detailed models of piezoceramic actuation of beams, *Journal of Intelligent Material Systems and Structures* 1 (1990) 4–25.
[9] C.K. Lee, Theory of laminated piezoelectric plates for the design of distributed sensors/actuators—part 1: governing equations and reciprocal relationships, *Journal of the Acoustical Society of America* 87 (1990) 1144–1158.
[10] J.H. Huang, T.L. Wu, Analysis of hybrid multilayered piezoelectric plates, *International Journal of Engineering Science* 34 (1996) 171–181.
[11] J.A. Mitchell, J.N. Reddy, A refined hybrid plate theory for composite laminates with piezoelectric laminae, *International Journal of Solids and Structures* 32 (1995) 2345–2367.
[12] R.C. Batra, X.Q. Liang, Finite dynamic deformations of smart structures, *Computational Mechanics* 20 (1997) 427–438.
[13] M.C. Ray, K.M. Rao, B. Samanta, Exact solution for static analysis of intelligent structures under cylindrical bending, *Computers and Structures* 47 (1993) 1031–1042.
[14] P. Heyliger, S. Brooks, Exact solutions for laminated piezoelectric plates in cylindrical bending, *Journal of Applied Mechanics* 63 (1996) 903–910.
[15] P. Heyliger, Static behavior of laminated elastic/piezoelectric plates, *AIAA Journal* 32 (1994) 2481–2484.
[16] P. Heyliger, Exact solutions for simply supported laminated piezoelectric plates, *Journal of Applied Mechanics* 64 (1997) 299–306.
[17] P. Bisegna, F. Maceri, An exact three-dimensional solution for simply supported rectangular piezoelectric plates, *Journal of Applied Mechanics* 63 (1996) 628–638.
[18] J.S. Lee, L.Z. Jiang, Exact electroelastic analysis of piezoelectric laminae via state space approach, *International Journal of Solids and Structures* 33 (1996) 977–990.
[19] J.S. Yang, R.C. Batra, X.Q. Liang, The cylindrical bending vibration of a laminated elastic plate due to piezoelectric actuators, *Smart Materials and Structures* 3 (1994) 485–493.
[20] R.C. Batra, X.Q. Liang, J.S. Yang, The vibration of a simply supported rectangular elastic plate due to piezoelectric actuators, *International Journal of Solids and Structures* 33 (1996) 1597–1618.
[21] S.S. Vel, R.C. Batra, Cylindrical bending of laminated plates with distributed and segmented piezoelectric actuators/sensors, *AIAA Journal* 38 (2000) 857–867.
[22] S.S. Vel, R.C. Batra, Three-dimensional analytical solutions for hybrid multilayered piezoelectric plates, *Journal of Applied Mechanics* 67 (2000) 558–567.

[23] S.S. Vel, R.C. Batra, Analysis of piezoelectric bimorphs and plates with segmented actuators, *Thin-walled Structures* 39 (2001) 23–44.
[24] P. Heyliger, S. Brooks, Free-vibration of piezoelectric laminates in cylindrical bending, *International Journal of Solids and Structures* 32 (1995) 2945–2960.
[25] P. Heyliger, D.A. Saravanos, Exact free-vibration analysis of laminated plates with embedded piezoelectric layers, *Journal of the Acoustical Society of America* 98 (1995) 1547–1557.
[26] C.T. Sun, X.D. Zhang, Use of thickness-shear mode in adaptive sandwich structures, *Smart Materials and Structures* 4 (1995) 202–206.
[27] V.A. Boriseiko, V.S. Martynenko, A.F. Ultiko, General theory of thin piezoceramic shells, *Vestnik Kiev Universiteta Matematika i Mekhanika* 25 (1983) 26–40 (in Ukrainian).
[28] Electro Ceramic Division, Data for Designers, Morgan Matroc, Bedford, OH, USA.
[29] X.D. Zhang, C.T. Sun, Formulation of an adaptive sandwich beam, *Smart Materials and Structures* 5 (1996) 814–823.
[30] X.D. Zhang, C.T. Sun, Analysis of a sandwich plate containing a piezoelectric core, *Smart Materials and Structures* 8 (1999) 31–40.
[31] A. Benjeddou, M.A. Trindade, R. Ohayon, A unified beam finite element model for extension and shear piezoelectric actuation mechanisms, *Journal of Intelligent Material Systems and Structures* 8 (1997) 1012–1025.
[32] M.A. Trindade, A. Benjeddou, R. Ohayon, Parametric analysis of the vibration control of sandwich beams through shear-based piezoelectric actuation, *Journal of Intelligent Material Systems and Structures* 10 (1999) 377–385.
[33] A. Benjeddou, J.-F. Deü, A two-dimensional closed-form solution for the free-vibrations analysis of piezoelectric sandwich plates, *International Journal of Solids and Structures* 39 (2002) 1463–1486.
[34] M.A. Trindade, A. Benjeddou, Hybrid active–passive damping treatments using viscoelastic and piezoelectric materials: review and assessment, *Journal of Vibration and Control* 8 (2002) 699–745.
[35] R.C. Batra, T.S. Geng, Comparison of active constrained layer damping by using extension and shear mode actuators, *Journal of Intelligent Material Systems and Structures* 13 (2002) 349–367.
[36] S.S. Vel, R.C. Batra, Exact solution for cylindrical bending of laminated plates with embedded shear actuators, *Smart Materials and Structures* 10 (2001) 240–251.
[37] S.S. Vel, R.C. Batra, Exact solution for rectangular sandwich plates with embedded piezoelectric Shear actuators, *AIAA Journal* 39 (2001) 1363–1373.
[38] C.J. Goh, T.K. Caughey, On the stability problem caused by finite actuator dynamics in the control of large space structures, *International Journal of Controls* 41 (1985) 787–802.
[39] J.L. Fanson, T.K. Caughey, Positive position feedback for large space structure, *AIAA Journal* 28 (1990) 717–724.
[40] M. Friswell, D.J. Inman, The relationship between positive position feedback and output feedback controllers, *Smart Materials and Structures* 8 (1999) 285–291.
[41] J.F. Nye, *Physical Properties of Crystals*, Oxford University Press, New York, 1985.
[42] H.F. Tiersten, *Linear Piezoelectric Plate Vibrations*, Plenum Press, New York, 1969.
[43] N.J. Pagano, Influence of shear coupling in cylindrical bending of anisotropic laminates, *Journal of Composite Materials* 4 (1970) 330–343.
[44] S.S. Vel, R.C. Batra, Three-dimensional exact solution for the vibration of functionally graded rectangular plates, *Journal of Sound and Vibration* 272 (2004) 703–730.
[45] Y.Y. Tang, A.K. Noor, K. Xu, Assessment of computational models for thermoelectroelastic multilayered plates, *Computers and Structures* 61 (1996) 915–933.
[46] ABAQUS Users Manual, Version 6.3, Hibbit, Karlsson & Sorensen, Inc., 2002.